



Three years of Ulysses dust data: 1993–1995

H. Krüger^{a,*}, E. Grün^a, M. Landgraf^a, M. Baguhl^a, S. Dermott^b, H. Fechtig^a,
B.A. Gustafson^b, D.P. Hamilton^c, M.S. Hanner^d, M. Horányi^c, J. Kissel^a,
B.A. Lindblad^f, D. Linkert^a, G. Linkert^a, I. Mann^g, J.A.M. McDonnell^h, G.E. Morfillⁱ,
C. Polanskey^d, G. Schwehm^j, R. Srama^a, H.A. Zook^k

^a Max-Planck-Institut für Kernphysik, 69029 Heidelberg, Germany

^b University of Florida, Gainesville, FL 32611, U.S.A.

^c University of Maryland, College Park, MD 20742-2421, U.S.A.

^d Jet Propulsion Laboratory, Pasadena, CA 91109, U.S.A.

^e Laboratory for Atmospheric and Space Physics, University of Colorado, Boulder, CO 80309, U.S.A.

^f Lund Observatory, 221 Lund, Sweden

^g Max-Planck-Institut für Aeronomie, 37191 Katlenburg-Lindau, Germany

^h University of Kent, Canterbury CT2 7NR, U.K.

ⁱ Max-Planck-Institut für Extraterrestrische Physik, 85748 Garching, Germany

^j ESTEC, 2200 AG Noordwijk, The Netherlands

^k NASA Johnson Space Center, Houston, TX 77058, U.S.A.

Received 9 April 1998; received in revised form 28 September 1998; accepted 2 October 1998

Abstract

The Ulysses spacecraft is orbiting the Sun on a highly inclined ellipse ($i = 79^\circ$). After its Jupiter flyby in 1992 at a heliocentric distance of 5.4 AU, the spacecraft reapproached the inner solar system, flew over the Sun's south polar region in September 1994, crossed the ecliptic plane at a distance of 1.3 AU in March 1995, and flew over the Sun's north polar region in July 1995. We report on dust impact data obtained with the dust detector onboard Ulysses between January 1993 and December 1995. We publish and analyse the complete data set of 509 recorded impacts of dust particles with masses between 10^{-16} g– 10^{-7} g. Together with 968 dust impacts from launch until the end of 1992 published earlier (Grün et al., 1995c), information about 1477 particles detected with the Ulysses sensor between October 1990 and December 1995 is now available. The impact rate measured between 1993 and 1995 stayed relatively constant at about 0.4 impacts per day and varied by less than a factor of ten. Most of the impacts recorded outside about 3.5 AU are compatible with particles of interstellar origin. Two populations of interplanetary particles have been recognized: big micrometer-sized particles close to the ecliptic plane and small sub-micrometer-sized particles at high ecliptic latitudes. The observed impact rate is compared with a model for the flux of interstellar dust particles which gives relatively good agreement with the observed impact rate. No change in the instrument's noise characteristics or degradation of the channeltron could be revealed during the three-year period. © 1999 Elsevier Science Ltd. All rights reserved.

1. Introduction

The Ulysses mission is exploring the solar system between 1 and 5.4 AU from the Sun over a wide range of ecliptic latitudes (-79° – $+79^\circ$). Ulysses carries a multi-coincidence impact ionization detector, which is nearly identical to the dust detector flown onboard the Galileo spacecraft. Detailed descriptions of the dust instruments onboard both spacecraft have been published by Grün et al. (1992a, b; 1995a). Early results on interplanetary dust obtained from both missions and dust measurements

achieved by Ulysses in the environment of Jupiter have been reported (Grün et al., 1992c, d; Grün, 1994). Unexpected intermittent streams of dust particles originating from the Jovian system and interstellar particles sweeping through the solar system were discovered by Ulysses (Grün et al., 1993). A detailed analysis of the complete Ulysses dust data has led to the identification of 'small' impacts that had been previously considered potential noise events (Baguhl et al., 1993).

Data from the dust instruments onboard both spacecraft—Ulysses and Galileo—have been used in various ways: asteroids and comets have been investigated as dust sources (Riemann and Grün, 1992; Hamilton and Burns, 1992; Grün et al., 1994a; Mann et al., 1996a); conse-

* Corresponding author. Fax: +49 6221 516 324; e-mail: krueger@galileo.mpi-hd.mpg.de

quences for the zodiacal light and other interplanetary meteoroid measurements have been considered (Mann et al., 1992; Mann and Grün, 1993; Mann et al., 1996b; Taylor et al., 1996); a detailed model of interplanetary meteoroid populations in the solar system has been developed (Divine, 1993; Divine et al., 1993; Grün and Staubach, 1996; Grün et al., 1997); the dust streams originating from the Jovian system have been analysed (Horányi et al., 1993a, b; Hamilton and Burns, 1993; Zook et al., 1996) and, finally, the properties of interstellar dust in the heliosphere have been investigated (Grün et al., 1994b; Baguhl et al., 1995a, b; 1996; Landgraf and Grün, 1998).

This is the fifth paper in a series dedicated to presenting both raw and reduced data obtained from the dust instruments onboard the Ulysses and Galileo spacecraft. Grün et al. (1995a; hereafter, Paper I) describe the reduction process of Ulysses and Galileo dust data. Papers II and III (Grün et al., 1995b, c) present the data sets from the initial three and two years of the Galileo and Ulysses missions, respectively. In the case of Ulysses the time period covered (Paper III) was October 1990–December 1992. In the current paper we extend the Ulysses data set from January 1993 until December 1995. In a companion paper (Krüger et al., 1998, Paper IV), we publish the Galileo data set for the same time period. The main data products are a table of the impact rate of all impacts determined from the particle accumulators and a table of both raw and reduced data of all dust impacts transmitted to Earth. The information presented in these papers is similar to data which we are submitting to the various data archiving centers (Planetary Data System, NSSDC, Ulysses Data Center, etc.). Electronic access to the data is also possible via the world wide web: <http://galileo.mpi-hd.mpg.de>.

This paper is organised similarly to Paper III. Section 2 gives a brief overview of the Ulysses mission and lists important mission events from 1993–95. A description of the Ulysses dust data set for this period is given in Section 3. Sections 4 and 5 analyse and discuss the new data set.

2. Mission and instrument operation

Ulysses was launched on 6 October 1990 and was brought onto a direct trajectory towards Jupiter. A swing-by manoeuvre at Jupiter on 8 February 1992 deflected the spacecraft into an orbit that is inclined by 79° to the ecliptic plane (Fig. 1). In October 1994 Ulysses passed the Sun's south polar region, then crossed the ecliptic plane again, this time at a perihelion distance of 1.3 AU on 12 March 1995 and flew over the Sun's north polar region in August 1995. In April 1998 the spacecraft crossed the ecliptic plane at its aphelion at 5.4 AU. Approximate orbital elements for the Ulysses trajectory that include the whole out-of-ecliptic part of its orbit, are given in Paper III.

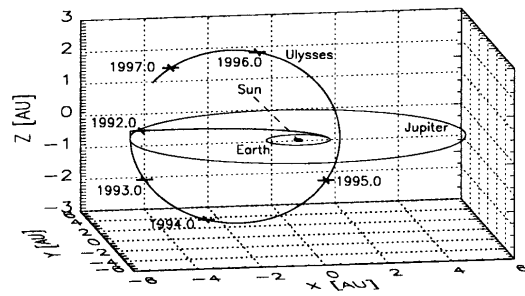


Fig. 1. Three-dimensional view of Ulysses' interplanetary trajectory from launch until the end of 1996 in ecliptic coordinates. The Sun is in the center. The orbits of Earth and Jupiter indicate the ecliptic plane. The initial trajectory of Ulysses was in the ecliptic plane. During Jupiter flyby in early 1992 Ulysses was brought into an orbit with 79° inclination that sent the spacecraft close to the ecliptic poles. Crosses mark the spacecraft position at the beginning of each year. Vernal equinox is to the right (positive x axis).

Ulysses is a spin-stabilized spacecraft with its spin axis pointing towards Earth. In Fig. 2 we show the deviation of the spin axis from the nominal Earth direction for the period 1993 to 1995 considered in this paper. Most of the time the axis pointing was within one degree of the Earth direction. This rather small deviation is negligible for the considerations in this paper. The Ulysses spacecraft and mission are explained in more detail by Wenzel et al. (1992). Details about the data transmission to Earth can also be found in Paper III.

The dust detector onboard Ulysses (GRU) has a 140° wide field of view. The instrument is mounted nearly at right angles (85°) to the antenna pointing direction (spacecraft spin axis). Therefore, the sensor is most sensitive to particles approaching from the plane perpendicular to the spacecraft–Earth direction. The

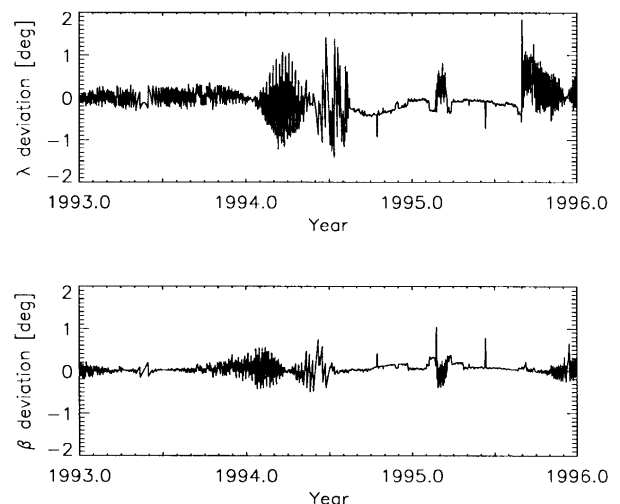


Fig. 2. Spacecraft attitude: deviation of the antenna pointing direction (i.e., negative spin axis) from the nominal Earth direction. The angles are given in ecliptic longitude (top) and latitude (bottom, equinox 1950.0).

rotation angle measures the sensor viewing direction at the time of a dust impact. During one spin revolution the rotation angle scans through a complete circle of 360° . The 0° rotation angle is defined to be the direction closest to ecliptic north. At high ecliptic latitudes, however, the sensor pointing at 0° rotation angle significantly deviates from the actual north direction. During the passages over the Sun's polar regions the sensor always scans through a plane tilted by about 30° from the ecliptic and all rotation angles lie close to the ecliptic plane (cf. Fig. 4 in Grün et al., 1997). A sketch of the viewing geometry can be found in Grün et al. (1993).

Table 1 lists significant mission and dust instrument events from 1993–95. Earlier events are only listed if especially significant. A comprehensive list of events from launch until the end of 1992 is given in Paper III. During the early phases of the mission the in-orbit noise characteristics of the instrument were investigated (Paper III). This led to a relatively noise-free configuration (hereafter called nominal configuration) for the instrument after 10 February 1992: channeltron voltage 1140 V (HV = 3); event definition status such that either the channeltron or the ion-collector channel can, independent of each other, start a measurement cycle (EVD = C, I); detection thresholds for ion-collector, channeltron and electron-channel set to the lowest levels and the detection threshold for the entrance grid set to the first digital step (SSEN = 0, 0, 0, 1). See Paper I for a description of these terms.

The operational configuration of the dust instrument was changed several times during noise tests: starting from the nominal configuration described above, all tests have been performed with the same instrument settings. During noise tests, the following changes of the instrument configuration were applied at one-hour intervals: (a) set the event definition status such that the channeltron, the ion collector and the electron-channel can initiate a measurement cycle (EVD = C, I, E); (b) set the thresholds for all channels to their lowest levels (SSEN = 0, 0, 0, 0); (c) reset the event definition status to its nominal configuration (EVD = C, I); (d) increase the channeltron high voltage by one digital step (HV = 4); (e) reset the channeltron high voltage and the detection thresholds to their nominal settings (HV = 3, SSEN = 0, 0, 0, 1). After step (e) the instrument is back in its nominal configuration. No detectable change in the noise behavior was revealed by the noise tests during the three years from 1993–95.

Spacecraft anomalies occurred five times between 1993 and 1995, and all scientific instruments onboard were switched off automatically for about one day during so-called DNELs (Disconnect all Non-Essential Loads). After each DNEL, the dust instrument was switched on again and was configured to its nominal operational mode.

The dust instrument has two heaters to allow for a

relatively stable operating temperature within the sensor. By heating one of the two or both heaters, three different heating power levels can be achieved (400, 800 or 1200 mW). One or both heaters were switched on most of the time, except close to the Sun between 5 February and 12 June 1995 when both were switched off. The heaters remained switched on during the DNELs. Table 1 lists the total heating powers provided by the heaters. The temperature of the dust sensor was between -20°C – $+15^\circ\text{C}$.

A timing error in the instrument electronics led to wrong spacecraft sector information for about 20% of the events in the data set published earlier (cf. Paper III, indicated by ROT = 999 in Table 4). The error was corrected by a reprogramming of the instrument on 30 April 1993.

After launch of Ulysses the sounder of the URAP instrument (Stone et al., 1992) emerged as a significant and unexpected noise source for the dust sensor. When the sounder was switched on after launch, sounder interference caused about 20% dead time (Paper III). With the sounder now usually being operated at a lower rate of about 2 min at 2 h intervals the dead time is reduced to about 2%. In a detailed investigation of the noise behavior of the Ulysses dust instrument Baguhl et al. (1993) showed that the noise rate measured during periods of sounder operation was correlated with the distance to, and the position of, the Sun with respect to the sensor-viewing direction: most noise events are triggered when the Sun shines directly into the sensor. On the other hand, when the spacecraft was at large heliocentric distances in 1993, the noise rate was extremely low, even during sounder operation periods.

In Fig. 3 we show the noise rate for the 1993–95 period. The upper panel shows the daily maxima, which are dominated by interference with the sounder. Since the sounder was operated for periods of only 2 min with quiet intervals of about 2 h, such high noise rates prevailed only during about 2% of the time, with the remaining 98% being free of sounder noise. In 1994 the maxima in the noise rate induced by the sounder began to increase significantly when Ulysses approached the inner solar system. The highest sounder noise rates occurred around perihelion passage in March 1995. From 12–22 July 1994 and 24 November–1 December 1994, the sounder was switched off and the noise level dropped to about 10 events per day. The noise during quiet times when the sounder was switched off is shown in the lower panel of Fig. 3. The average was about 20 events per day which shows that the dust instrument was not affected by dead time caused by random noise events during 98% of the time.

3. Impact events

Impact events are classified into four classes and six ion charge amplitude ranges which lead to 24 individual

Table 1

Ulysses mission and dust detector (GRU) configuration, tests and other events. Only selected events before 1993 are given. See Section 2 for details

Year–day	Date	Time	Event
90–279	06.10.90		Ulysses launch
91–154	03.06.91	18:13	GRU heater on: 1200 mW
92–041	10.02.92	17:00	GRU nominal configuration: HV = 3, EVD = C, I, SSEN = 0001
93–045	14.02.93	06:53	Ulysses DNEL #2
93–045	14.02.93	22:50	GRU on, nominal configuration
93–120	30.04.93	02:46	GRU new program (FN7 data) load
93–126	06.05.93	23:07	GRU start new program
93–196	15.07.93	02:00	GRU noise test
93–206	25.07.93	01:00	GRU HV = 4
93–211	30.07.93	06:03	GRU HV = 3
93–221	09.08.93	12:17	Ulysses DNEL #3
93–223	11.08.93	22:36	GRU on
93–224	12.08.93	07:43	GRU nominal configuration
93–231	19.08.93	01:59	GRU noise test
93–259	16.09.93	11:59	GRU noise test
93–287	14.10.93	18:59	GRU noise test
93–315	11.11.93	19:59	GRU noise test
93–331	27.11.93	23:41	Ulysses DNEL #4
93–332	28.11.93	15:21	GRU on
93–332	28.11.93	22:58	GRU nominal configuration
93–343	09.12.93	18:00	GRU noise test
94–006	06.01.94	16:00	GRU noise test
94–034	03.02.94	14:59	GRU noise test
94–062	03.03.94	07:00	GRU noise test
94–090	31.03.94	08:45	GRU noise test
94–118	28.04.94	07:30	GRU noise test
94–146	26.05.94	05:00	GRU noise test
94–174	22.06.94	06:00	GRU noise test
94–202	21.07.94	03:59	GRU noise test
94–230	18.08.94	02:59	GRU noise test
94–258	15.09.94	00:00	GRU noise test
94–276	03.10.94		Ulysses South polar pass (lat. -79° , 2.1 AU)
94–281	08.10.94	00:30	GRU heater: 800 mW
94–283	10.10.94	18:45	Ulysses DNEL #5
94–284	11.10.94	23:06	GRU on
94–285	12.10.94	04:17	GRU nominal configuration
94–286	13.10.94	19:59	GRU noise test
94–314	10.11.94	04:59	GRU noise test
94–341	08.12.94	23:59	GRU noise test
94–005	05.01.95	00:00	GRU noise test
95–003	02.02.95	01:59	GRU noise test
95–036	05.02.95	01:24	GRU heater off
95–071	12.03.95	12:01	Ulysses ecliptic plane crossing and perihelion (1.3 AU)
95–152	01.06.95	03:59	GRU noise test
95–163	12.06.95	03:31	GRU heater on: 400 mW
95–180	29.06.95	03:59	GRU noise test
95–208	27.07.95	04:00	GRU noise test
95–216	04.08.95	00:51	GRU heater: 800 mW
95–231	19.08.95		Ulysses North polar pass (lat. $+79^\circ$, 2.1 AU)
95–236	24.08.95	15:59	GRU noise test
95–264	21.09.95	18:59	GRU noise test
95–292	19.10.95	19:59	GRU noise test
95–300	27.10.95	16:23	GRU heater: 1200 mW
95–320	16.11.98	09:59	GRU noise test
95–344	10.12.95	15:55	Ulysses DNEL #6
95–344	10.12.95	21:28	GRU on
95–346	12.12.95	08:54	GRU nominal configuration
95–348	14.12.95	15:00	GRU noise test

Abbreviations used: DNEL: Disconnect non-essential loads (i.e., all scientific instruments); HV: channeltron high voltage step; EVD: event definition, ion- (I), channeltron- (C), or electron-channel (E); SSEN: detection thresholds, ICP, CCP, ECP and PCP.

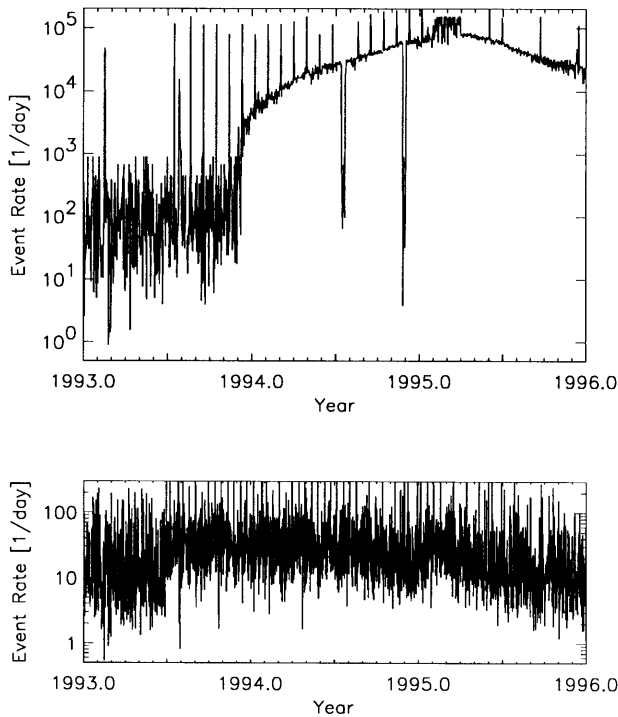


Fig. 3. Noise rate (class 0 events) detected with the dust instrument. Upper panel: Daily maxima in the noise rate (determined from the AC01 accumulator). The sounder was operated for only 2% of the total time, and the daily maxima are dominated by sounder noise. Sharp spikes are caused by periodic noise tests and short periods of re-configuration after DNELs (cf. Table 1). From 12–22 Jul. 1994 and 24 Nov. to 1 Dec. 1994 the sounder was not operated, which reduced the maximum noise by several orders of magnitude. Lower panel: Noise rate detected during quiet intervals when the sounder was switched off, which was the case about 98% of the time (one-day average calculated from the number of AC01 events for which the complete information has been transmitted to Earth).

categories. In addition, the instrument has 24 accumulators with one accumulator belonging to one individual category. Class 3, our highest class, are real dust impacts and class 0 are noise events. Depending upon the noise of the charge measurements, classes 1 and 2 can be true dust impacts or noise events. This classification scheme for impact events has been described in Paper I and this scheme is still valid for the Ulysses dust instrument. In contrast to the Galileo dust instrument which had to be reprogrammed because of the low data transmission capabilities of the Galileo spacecraft, no such reprogramming was necessary for Ulysses. Most of the data processing for Ulysses is done on the ground.

Between 1 January 1993 and 31 December 1995 the complete data (sensor orientation, charge amplitudes, charge rise times, etc.) of 72,809 events including 509 dust impacts were transmitted to Earth. Table 2 lists the number of all dust impacts counted with the 24 accumulators of the dust instrument. ‘AC x : y ’ refers to class number ‘ x ’ and amplitude range ‘ y ’ (for a detailed description of the accumulator categories see Paper I). As discussed

in the previous section, most noise events were recorded during the short time periods when either the sounder of the URAP instrument was operating (cf. Paper III) or the dust instrument was configured to its high sensitive state for noise tests, or both. During these periods many events were only counted by one of the 24 accumulators because their full information was overwritten before the data could be transmitted to Earth (see bottom of Table 2). Since the dust impact rate was low during times surrounding these periods, it is expected that only a few true dust impacts were lost.

Two particles in AC32 and AC33 (days 93–154, 21:01 h and 93–319, 15:31 h), respectively, were detected in a gap of several hours when no data could be transmitted to Earth, and their full information had to be taken from the instrument memory (FN7, cf. Grün et al., 1992a). Before and after these gaps the sounder was operated for about 2 min at 2 h intervals and we assume that it was operated with the same frequency in the gap. Due to these long quiet intervals between sounder operation it is rather unlikely that the two events occurred when the sounder was active. Even in such a case these are still very likely true dust impacts because the sounder noise usually affects only the lowest ion amplitude range (AR1).

All 509 dust impacts detected between 1993 and 1995 for which the complete information exists are listed in Table 3. Dust particles are identified by their sequence number and their impact time (first two columns). The event category—class (CLN) and amplitude range (AR)—are given in the third and fourth columns. Raw data as transmitted to Earth are shown in the next columns: sector value (SEC) which is the spacecraft spin orientation at the time of impact, impact charge numbers (IA, EA, CA) and rise times (IT, ET), time difference and coincidence of electron and ion signals (EIT, EIC), coincidence of ion and channeltron signal (IIC), charge reading at the entrance grid (PA) and time (PET) between this signal and the impact. Then the instrument configuration is given: event definition (EVD), charge sensing thresholds (ICP, ECP, CCP, PCP) and channeltron high voltage step (HV). Compare Paper I for further explanation of the instrument parameters.

The next four columns in Table 3 give information about Ulysses’ orbit: heliocentric distance (R), ecliptic longitude and latitude (LON, LAT) and distance from Jupiter (D_{Jup}). The next column gives the rotation angle (ROT) as described in Section 2. Whenever this value is unknown, ROT is arbitrarily set to 999. This occurs 14 times. Then follows the pointing direction of the dust instrument at the time of particle impact in ecliptic longitude and latitude (S_{LON} , S_{LAT}). When ROT is not valid S_{LON} and S_{LAT} are useless and are also set to 999. Mean impact velocity (V) and velocity error factor (VEF , i.e., multiply or divide stated velocity by VEF to obtain upper or lower limits) as well as mean particle mass (M) and

Table 2

Overview of dust impacts accumulated with the Ulysses dust detector between 1 January 1993 and 31 December 1995. Switch-on of the instrument is indicated by horizontal lines. The heliocentric distance R , the lengths of the time interval Δt (days) from the previous table entry, and the corresponding numbers of impacts are given for the 24 accumulators. The accumulators are arranged with increasing signal amplitude ranges (AR), with four event classes for each amplitude range (CLN = 0, 1, 2, 3); e.g., AC31 means counter for AR = 1 and CLN = 3. The Δt in the first line (93–001) is the time interval counted from the last entry in Table 3 in Paper III. The totals of counted impacts*, of impacts with complete data, and of all events (noise plus impact events) for the entire period are also given

Date	Time (h)	R (AU)	Δt (d)	AC 01*	AC 11*	AC 21	AC 31	AC 02*	AC 12	AC 22	AC 32	AC 03	AC 13	AC 23	AC 33	AC 04	AC 14	AC 24	AC 34	AC 05	AC 15	AC 25	AC 35	AC 06	AC 16	AC 26	AC 36
93–001	02:08	5.065	2.1	—	—	—	—	—	—	—	—	—	—	—	—	—	—	—	—	—	—	—	—	—	—	—	—
93–008	09:24	5.049	7.3	—	1	—	—	—	—	—	2	—	—	—	2	—	—	—	—	—	—	—	—	—	—	—	—
93–016	02:51	5.028	7.7	1	—	—	—	1	—	—	2	—	—	—	—	—	—	—	—	—	—	—	—	—	—	—	—
93–023	03:00	5.011	7.0	1	—	—	—	—	1	—	—	—	—	—	—	—	—	—	—	—	—	—	—	—	—	—	—
93–030	07:15	5.001	7.2	—	—	—	—	—	—	—	1	—	—	—	1	—	—	—	—	—	—	—	—	—	—	—	—
93–044	18:50	4.967	14.5	1	1	—	1	—	1	—	1	—	—	—	—	—	—	—	—	—	—	—	—	—	—	—	—
93–045	14:53	4.952	0.8	-----																							
93–053	02:13	4.931	7.5	—	—	—	—	1	—	—	2	—	1	—	2	—	—	—	—	—	—	—	—	—	—	—	—
93–060	06:07	4.929	7.2	—	—	—	—	—	—	—	—	—	—	—	—	—	—	—	—	—	—	—	—	—	—	—	—
93–068	05:29	4.888	8.0	2	—	—	—	—	—	—	—	—	—	—	—	—	—	—	—	—	—	—	—	—	—	—	—
93–076	01:48	4.889	7.8	1	—	—	—	1	—	—	2	—	—	—	1	—	—	—	—	—	—	—	—	—	—	—	—
93–083	03:48	4.870	7.1	1	—	—	—	—	—	—	2	—	—	—	1	—	—	—	—	—	—	—	—	—	—	—	—
93–090	04:04	4.852	7.0	—	1	—	—	1	—	—	3	—	—	—	1	—	—	—	—	—	—	—	—	—	—	—	—
93–098	02:25	4.796	7.9	1	—	—	—	—	2	—	1	—	—	—	—	—	—	—	—	—	—	—	—	—	—	—	—
93–105	04:50	4.810	7.1	1	1	—	—	—	1	—	—	—	—	—	—	—	—	—	—	—	—	—	—	—	—	—	—
93–113	00:08	4.788	7.8	—	1	—	—	—	—	—	1	—	—	—	—	—	—	—	—	—	—	—	—	—	—	—	—
93–120	00:37	4.768	7.0	1	—	—	—	—	—	—	2	—	—	—	—	—	—	—	1	—	—	—	—	—	—	—	—
93–127	01:10	4.747	7.0	1	—	—	—	—	—	1	—	—	—	—	—	—	—	—	—	—	—	—	—	—	—	—	—
93–134	04:48	4.726	7.2	—	—	—	1	—	—	—	—	—	—	—	—	—	—	—	—	—	—	—	—	—	—	—	—
93–142	00:32	4.702	7.8	—	—	—	—	—	—	—	—	—	—	—	—	—	—	—	—	—	—	—	—	—	—	—	—
93–149	01:25	4.680	7.0	—	—	—	—	—	1	—	—	—	—	—	—	—	—	—	—	—	—	—	—	—	—	—	—
93–156	02:37	4.597	7.1	1	—	—	—	—	—	—	—	—	—	—	1	—	—	—	—	—	—	—	—	—	—	—	—
93–164	01:55	4.633	8.0	—	2	—	—	—	—	—	—	—	—	—	1	—	—	—	—	—	—	—	—	—	—	—	—
93–171	02:42	4.540	7.0	—	—	—	—	—	—	—	—	—	—	—	—	—	—	—	—	—	—	—	—	—	—	—	—
93–179	01:33	4.583	8.0	—	—	—	—	—	—	—	1	—	—	—	1	—	—	—	—	—	—	—	—	—	—	—	—
93–187	11:29	4.476	8.4	—	—	—	—	—	—	—	—	—	—	—	—	—	—	—	—	—	—	—	—	—	—	—	—
93–195	01:06	4.529	7.6	—	—	—	—	—	—	—	1	—	—	—	—	—	—	—	—	—	—	—	—	—	—	—	—
93–202	01:49	4.505	7.0	—	—	—	—	—	1	—	—	—	—	—	—	—	—	—	—	—	—	—	—	—	—	—	—
93–210	00:09	4.476	7.9	—	—	—	—	—	—	—	—	—	—	—	1	—	—	—	—	—	—	—	—	—	—	—	—
93–217	00:11	4.451	7.0	—	—	—	—	—	1	—	—	—	—	—	1	—	—	—	—	—	—	—	—	—	—	—	—
93–224	06:14	4.424	7.3	1	—	—	—	—	—	—	—	—	—	—	1	—	—	—	—	—	—	—	—	—	—	—	—
93–225	06:29	4.421	1.0	-----																							
93–233	01:23	4.392	7.8	1	—	—	—	—	—	—	1	—	—	—	—	—	—	—	—	—	—	—	—	—	—	—	—
93–241	03:55	4.361	8.1	1	—	—	—	—	—	1	1	—	—	—	2	—	—	—	—	—	—	—	—	—	—	—	—
93–249	02:41	4.210	7.9	1	—	—	1	—	—	—	—	—	—	—	—	—	—	—	—	—	—	—	—	—	—	—	—
93–257	01:23	4.299	7.9	—	—	—	—	1	—	—	—	—	—	—	—	—	—	—	—	—	—	—	—	—	—	—	—
93–265	10:20	4.266	8.4	—	—	—	—	—	1	—	1	—	—	—	—	—	—	—	—	—	—	—	—	—	—	—	—
93–273	01:04	4.235	7.6	2	—	—	—	—	—	2	—	—	—	—	—	—	—	—	—	—	—	—	—	—	—	—	—
93–281	01:15	4.202	8.0	—	—	—	—	—	1	1	—	—	—	—	1	—	—	—	—	—	—	—	—	—	—	—	—
93–288	02:55	4.021	7.1	1	—	—	—	1	—	—	—	—	—	—	—	—	—	—	—	—	—	—	—	—	—	—	—
93–296	06:11	4.138	8.1	—	1	—	—	—	1	—	—	—	—	—	—	—	—	—	—	—	—	—	—	1	—	—	—
93–304	00:43	4.105	7.8	—	—	—	—	—	—	—	1	—	—	—	2	—	—	—	1	—	—	—	—	—	—	—	—
93–312	02:43	3.898	8.1	1	—	—	—	—	—	—	—	—	—	—	1	—	—	—	—	—	—	—	—	—	—	—	—
93–320	03:49	4.034	8.0	2	—	—	—	—	—	2	—	—	—	—	—	—	—	—	—	—	—	—	—	—	—	—	—
93–331	17:21	3.792	11.6	4	—	—	—	—	1	—	1	—	—	—	1	—	1	—	—	—	—	—	—	—	—	—	—

continued

Table 2—continued

Date	Time (h)	R (AU)	Δt (d)	AC 01*	AC 11*	AC 21	AC 31	AC 02*	AC 12	AC 22	AC 32	AC 03	AC 13	AC 23	AC 33	AC 04	AC 14	AC 24	AC 34	AC 05	AC 15	AC 25	AC 35	AC 06	AC 16	AC 26	AC 36
93-332	17:22	3.786	1.0	—	—	—	—	—	—	—	—	—	—	—	—	—	—	—	—	—	—	—	—	—	—	—	—
93-340	01:29	3.943	7.3	—	—	—	—	—	—	—	—	—	—	—	—	—	—	—	—	—	—	—	—	—	—	—	—
93-348	00:46	3.906	8.0	1	—	—	—	1	—	—	—	—	—	—	2	—	—	—	1	—	—	—	—	—	—	—	—
93-356	00:16	3.868	8.0	—	—	—	—	—	—	—	—	—	—	—	1	—	—	—	—	—	—	—	—	—	—	—	—
93-363	00:49	3.834	7.0	—	—	—	—	—	—	—	—	—	—	—	—	—	—	—	—	—	—	—	—	—	—	—	—
94-006	01:02	3.795	8.0	1	1	—	—	—	—	—	—	—	—	—	2	—	—	—	—	—	—	—	—	—	—	—	—
94-014	01:59	3.755	8.0	—	—	—	—	—	—	—	1	—	—	—	1	—	—	—	—	—	—	—	—	—	—	—	—
95-022	00:58	3.715	8.0	3	—	—	1	—	—	—	—	—	—	—	—	—	—	—	1	—	—	—	—	—	—	—	—
94-030	00:15	3.674	8.0	2	—	—	—	—	—	—	1	—	—	—	—	—	—	—	—	—	—	—	—	—	—	—	—
94-037	02:40	3.614	7.1	—	—	—	—	—	—	—	—	—	—	—	3	—	—	—	—	—	—	—	—	—	—	—	—
94-045	00:18	3.596	7.9	1	—	—	—	—	1	—	—	—	—	—	1	—	—	—	—	—	—	—	—	—	—	—	—
94-052	00:41	3.559	7.0	—	—	—	—	—	—	—	—	—	—	—	—	—	—	—	—	—	—	—	—	—	—	—	—
94-060	01:07	3.516	8.0	1	—	—	—	—	—	—	—	—	—	—	—	—	—	—	—	—	—	—	—	—	—	—	—
94-068	00:22	3.473	8.0	—	—	—	—	—	—	—	—	—	—	—	1	—	—	—	—	—	—	—	—	—	—	—	—
94-075	00:42	3.434	7.0	1	—	—	—	—	—	—	—	—	—	—	1	—	—	—	—	—	—	—	—	—	—	—	—
94-083	00:55	3.389	8.0	1	—	—	—	—	—	—	—	—	—	—	—	—	—	—	—	—	—	—	—	—	—	—	—
94-090	01:14	3.350	7.0	4	—	—	1	—	1	—	—	—	1	—	—	—	—	—	—	—	—	—	—	—	—	—	—
94-098	01:19	3.304	8.0	1	—	—	—	—	—	—	—	—	1	—	—	—	—	—	—	—	—	—	—	—	—	—	—
94-106	00:45	3.257	8.0	2	—	—	—	1	—	—	—	—	—	—	1	—	—	—	—	—	—	—	—	—	—	—	—
94-113	00:46	3.216	7.0	2	—	—	—	—	—	—	—	—	—	1	—	—	—	—	—	—	—	—	—	—	—	—	—
94-124	00:05	3.150	11.0	1	—	—	—	—	—	—	—	—	1	—	—	—	—	—	—	—	—	—	—	1	—	—	—
94-131	00:15	3.108	7.0	1	—	—	—	—	—	—	—	—	—	—	—	—	—	—	—	—	—	—	—	—	—	—	—
94-138	01:26	3.065	7.0	1	—	—	—	—	—	—	—	—	—	—	1	—	—	—	—	—	—	—	—	—	—	—	—
94-146	00:26	3.016	8.0	—	—	—	—	2	1	—	—	—	—	—	—	—	—	—	—	—	—	—	—	—	—	—	—
94-154	00:44	2.966	8.0	—	—	—	—	—	—	—	—	—	—	—	2	—	—	—	—	—	—	—	—	—	—	—	—
94-162	00:27	2.915	8.0	2	—	—	—	—	—	1	—	—	—	—	—	—	—	—	—	—	—	—	—	—	—	—	—
94-169	23:56	2.728	8.0	1	—	—	—	1	—	—	—	—	—	—	—	—	—	—	—	—	—	—	—	—	—	—	—
94-177	00:04	2.818	7.0	1	—	—	—	—	1	—	—	—	—	—	1	—	—	—	—	—	—	—	—	—	—	—	—
94-184	00:12	2.773	7.0	4	—	—	1	1	—	—	1	—	—	—	1	—	—	—	—	—	—	—	—	—	—	—	—
94-192	00:11	2.720	8.0	3	1	—	—	—	1	—	—	—	—	—	—	—	—	—	—	—	—	—	—	—	—	—	—
94-199	02:39	2.506	7.1	1	—	—	—	1	2	—	—	—	—	—	1	—	—	—	—	—	—	—	—	—	—	—	—
94-207	00:07	2.619	7.9	3	—	—	—	—	—	—	—	—	—	—	1	—	—	—	—	—	—	—	—	—	—	—	—
94-214	00:09	2.572	7.0	—	—	—	1	—	1	—	—	—	—	—	—	—	—	—	—	—	—	—	—	—	—	—	—
94-221	00:43	2.524	7.0	—	—	—	—	—	1	—	—	—	—	—	—	—	—	—	—	—	—	—	—	—	—	—	—
94-229	00:55	2.469	8.0	3	1	—	—	—	—	—	—	—	—	—	—	—	—	—	—	—	—	—	—	1	—	—	—
94-237	00:24	2.413	8.0	2	—	—	1	1	1	—	1	—	—	—	—	—	—	—	—	—	—	—	—	—	—	—	—
94-245	00:24	2.357	8.0	3	—	—	1	—	—	—	—	—	—	—	—	—	—	—	—	—	—	—	—	—	—	—	—
94-253	00:24	2.301	8.0	—	—	—	—	—	1	—	—	—	—	—	2	—	—	—	—	—	—	—	—	—	—	—	—
94-261	00:02	2.245	8.0	1	—	—	1	—	—	—	—	—	—	—	1	—	—	—	—	—	—	—	—	—	—	—	—
94-268	00:30	2.195	7.0	1	—	—	—	—	—	—	1	—	—	—	—	—	—	—	—	—	—	—	—	—	—	—	—
94-276	00:00	1.895	8.0	1	—	—	—	—	—	—	1	—	1	—	—	—	—	—	—	—	—	—	—	—	—	—	1
94-283	15:14	2.084	7.6	4	—	—	—	1	—	—	—	—	—	—	1	—	—	—	—	—	—	—	—	—	—	—	—
94-285	23:58	1.816	2.4	—	—	—	—	—	—	—	—	—	—	—	—	—	—	—	—	—	—	—	—	—	—	—	—
94-293	00:02	2.018	7.0	1	1	—	1	—	—	—	—	—	—	—	1	—	—	—	1	—	—	—	—	—	—	—	—
94-301	00:16	1.962	8.0	1	—	—	—	—	—	—	2	—	—	—	1	—	—	—	—	—	—	—	—	—	—	—	—
94-309	00:01	1.906	8.0	5	—	—	—	—	2	—	1	—	—	1	—	—	—	—	—	—	—	—	—	—	—	—	—
94-317	00:02	1.851	8.0	5	—	—	—	—	1	—	1	—	—	—	—	—	—	—	—	—	—	—	—	—	—	—	—
94-324	00:36	1.804	7.0	2	—	—	1	—	—	—	—	—	—	—	—	—	—	—	1	—	—	—	—	—	—	—	—
94-331	06:16	1.755	7.2	1	—	—	—	1	1	—	—	—	—	—	—	—	—	—	—	1	—	—	—	—	—	—	—
94-339	01:47	1.705	7.8	1	—	—	—	—	1	—	1	—	—	—	1	—	—	1	—	—	—	—	—	—	—	—	—

continued

Table 2—*continued*

<i>Date</i>	<i>Time</i> (h)	<i>R</i> (AU)	Δt (d)	AC 01*	AC 11*	AC 21	AC 31	AC 02*	AC 12	AC 22	AC 32	AC 03	AC 13	AC 23	AC 33	AC 04	AC 14	AC 24	AC 34	AC 05	AC 15	AC 25	AC 35	AC 06	AC 16	AC 26	AC 36
94-347	00:10	1.655	7.9	3	—	—	—	1	—	—	—	—	1	—	1	—	—	—	—	—	—	—	—	—	—	—	—
94-354	00:44	1.613	7.0	1	—	—	—	1	—	—	—	1	—	—	—	—	—	—	—	—	—	—	—	—	1	—	—
94-362	00:00	1.314	8.0	1	—	—	—	1	—	—	—	—	—	—	—	—	—	1	1	—	—	—	—	—	—	—	—
95-004	01:17	1.529	7.1	—	—	—	—	1	—	—	—	—	—	—	—	—	—	—	—	—	—	—	—	—	—	—	—
95-012	00:02	1.488	7.9	1	—	—	—	—	1	—	—	—	—	1	—	—	—	—	—	1	—	—	—	—	—	—	—
95-019	23:57	1.442	8.0	3	—	—	—	1	—	—	—	—	—	—	—	—	—	1	1	—	—	—	—	—	—	—	—
95-027	00:04	1.423	7.0	5	—	—	—	—	—	—	—	—	—	—	1	—	—	—	—	—	—	—	—	—	—	—	1
95-034	23:59	1.382	8.0	5	—	—	—	—	—	1	—	—	—	—	—	—	—	—	—	—	—	—	—	—	—	—	—
95-042	01:28	1.375	7.1	3	—	—	—	—	—	—	1	—	—	—	—	—	—	—	—	—	—	—	—	—	—	—	—
95-050	01:03	1.357	8.0	2	—	—	—	—	—	—	—	—	—	—	—	—	—	—	—	—	1	—	—	—	—	—	—
95-058	00:57	1.346	8.0	5	—	—	—	1	—	—	1	1	—	—	1	—	1	—	—	—	—	—	—	—	—	—	—
95-066	00:01	1.340	8.0	7	—	1	—	—	—	—	—	—	—	—	1	—	2	—	—	—	1	—	—	—	—	—	—
95-073	00:41	1.340	7.0	11	—	—	—	2	—	—	—	—	1	—	1	—	—	—	1	—	—	1	1	—	—	—	—
95-080	01:36	1.346	7.0	7	—	—	—	—	—	—	—	—	—	1	—	—	—	—	—	—	—	—	—	—	1	—	—
95-088	00:29	1.358	8.0	6	—	—	—	3	—	—	—	—	—	—	1	—	—	—	—	—	—	—	—	—	—	—	2
95-095	00:30	1.373	7.0	9	—	1	—	—	—	—	—	—	—	—	1	—	—	—	—	—	—	1	1	—	—	—	—
95-103	00:08	1.395	8.0	8	—	—	—	—	—	—	—	—	—	—	2	—	—	—	—	—	—	—	—	—	1	—	—
95-111	00:00	1.476	8.0	4	—	—	—	—	1	—	—	—	—	—	—	—	—	—	—	—	—	—	—	—	—	—	—
95-119	00:15	1.456	8.0	3	1	—	—	—	—	—	—	1	—	—	—	—	—	—	—	—	—	—	—	—	—	—	—
95-127	00:30	1.493	8.0	—	—	—	1	—	—	—	—	—	—	—	—	—	—	—	—	—	—	—	—	—	—	—	—
95-135	00:11	1.534	8.0	2	1	—	1	—	—	—	—	—	—	—	—	—	—	—	1	—	—	—	—	—	—	—	—
95-142	00:35	1.572	7.0	5	—	—	—	—	—	—	—	—	—	—	—	—	—	—	—	—	—	—	—	—	—	—	—
95-150	00:51	1.619	8.0	1	—	—	—	1	—	—	—	—	—	—	—	—	—	—	—	—	—	—	—	—	—	—	—
95-158	01:05	1.667	8.0	2	—	—	—	—	—	—	—	—	—	—	1	—	—	—	—	—	—	—	—	—	—	—	—
95-166	01:25	1.718	8.0	1	—	—	—	—	—	—	1	—	—	—	—	—	—	—	—	—	—	—	—	—	—	—	—
95-174	01:40	1.770	8.0	2	—	—	—	—	—	—	—	—	—	—	—	—	—	—	—	—	—	—	—	—	—	—	—
95-182	01:15	1.824	8.0	2	—	—	—	—	—	—	—	—	—	—	—	—	—	—	—	—	—	—	—	—	—	—	—
95-189	01:43	1.872	7.0	—	—	—	2	1	—	—	—	—	—	—	—	—	—	—	—	—	—	—	—	—	—	—	—
95-197	01:05	1.927	8.0	—	—	—	—	—	—	—	1	—	—	—	—	—	—	—	—	—	—	—	—	—	—	—	—
95-204	01:51	1.976	7.0	3	—	—	—	—	—	—	—	—	—	—	—	1	—	—	—	—	—	—	—	—	—	—	—
95-212	00:07	2.032	7.9	2	1	—	—	1	—	—	—	—	1	—	—	—	—	—	—	—	—	—	—	—	—	—	—
95-219	00:07	2.082	7.0	1	—	—	—	3	—	—	1	—	—	—	—	—	—	—	—	—	—	—	—	—	—	—	—
95-226	01:16	2.131	7.0	2	—	—	—	1	—	—	—	—	—	—	—	—	—	—	—	—	—	—	—	—	—	—	—
95-233	01:42	2.181	7.0	4	—	—	—	1	—	—	—	—	—	—	—	—	—	—	—	—	—	—	—	—	—	—	—
95-240	23:59	2.450	7.9	3	—	—	—	—	—	—	—	—	—	—	—	—	—	—	—	—	—	—	—	—	—	—	—
95-248	00:49	2.287	7.0	2	1	—	—	—	—	—	—	—	—	—	—	—	—	—	—	—	—	1	—	—	—	—	—
95-255	01:18	2.336	7.0	1	—	—	—	—	—	—	—	—	—	—	—	—	—	—	—	—	—	—	—	—	—	—	—
95-262	01:50	2.385	7.0	1	—	—	—	—	—	—	—	—	1	1	—	—	—	—	—	—	—	—	—	—	—	—	—
95-270	00:19	2.441	7.9	3	—	—	—	—	—	—	1	—	1	—	—	—	—	—	—	—	—	—	—	—	—	—	—
95-277	00:19	2.489	7.0	1	—	—	—	—	—	—	—	—	—	—	—	—	—	—	—	—	—	—	—	—	—	—	—
95-284	01:14	2.538	7.0	2	—	—	—	—	—	—	—	—	—	—	—	—	—	—	—	—	—	—	—	—	—	—	—
95-292	00:08	2.592	8.0	1	—	—	—	—	—	—	—	—	—	—	—	—	—	—	—	—	—	—	—	—	—	—	—
95-299	00:27	2.640	7.0	2	—	—	—	1	—	—	—	—	—	—	2	—	—	—	—	—	—	—	—	—	—	—	—
95-306	01:38	2.687	7.0	3	—	—	—	—	—	—	—	—	—	—	—	—	—	—	—	—	—	—	—	—	—	—	—
95-313	01:38	2.733	7.0	1	—	—	—	—	—	—	—	—	—	—	—	—	—	—	—	—	—	—	—	—	—	—	—
95-320	03:37	2.780	7.1	3	—	—	—	—	—	—	—	—	—	—	1	—	—	—	—	—	—	—	—	—	—	—	—
95-328	01:21	2.831	7.9	1	—	—	—	2	—	—	—	—	—	—	—	—	—	—	—	—	—	—	—	—	—	—	—
95-335	02:38	3.146	7.1	—	—	—	—	—	—	—	—	—	—	—	—	—	—	—	—	—	—	—	—	—	—	—	—
95-344	13:11	2.937	9.4	1	—	—	1	—	—	—	—	—	—	—	—	—	—	—	—	—	—	—	—	—	—	—	—
95-345	00:05	2.941	0.5	—	—	—	—	—	—	—	—	—	—	—	—	—	—	—	—	—	—	—	—	—	—	—	—

continued

Table 2—continued

Date	Time (h)	R (AU)	Δt (d)	AC 01*	AC 11*	AC 21	AC 31	AC 02*	AC 12	AC 22	AC 32	AC 03	AC 13	AC 23	AC 33	AC 04	AC 14	AC 24	AC 34	AC 05	AC 15	AC 25	AC 35	AC 06	AC 16	AC 26	AC 36	
95–352	01:00	2.985	7.0	1	—	—	—	—	—	—	—	—	—	—	—	1	—	—	—	—	—	—	—	—	—	—	—	—
95–360	01:15	3.035	8.0	1	—	—	—	1	—	—	—	—	—	—	—	—	—	—	—	—	—	—	—	—	—	—	—	—
Impacts (counted)				235*	17*	1	18	40*	30	5	47	3	9	6	63	0	4	3	12	0	3	2	5	0	3	0	4	
Impacts (complete data)				235	17	1	18	40	30	5	47	2	9	6	63	0	4	3	12	0	3	2	5	0	3	0	4	
All events (complete data)				68176	3676	1	18	738	30	5	47	3	9	6	63	1	4	3	12	0	3	2	5	0	3	0	4	

* Entries for AC01, AC11 and AC02 are the number of impacts with complete data. Due to the noise contamination of these three categories the number of impacts cannot be determined from the accumulators. The method to separate dust impacts from noise events in these three categories has been given by Baguhl et al. (1993).

mass error factor (*MEF*) are given in the last columns. For *VEF* > 6, both velocity and mass values should be discarded. This occurs for 48 impacts. No intrinsic dust charge values are given (see Svestka et al., 1996 for a detailed analysis).

4. Analysis

The positive impact charge measured on the ion collector, Q_1 , is the most important impact parameter determined by the dust instrument because of its relative insensitivity to noise. In Fig. 4 we show the distribution of Q_1 for all dust particles detected between 1993–95. Ion impact charges have been detected over the entire range of six orders of magnitude in impact charge that can be measured by the dust instrument. About 1% of all impacts are close to the saturation limit of $Q_1 \sim 10^{-8}$ C and may thus constitute lower limits of the actual impact charges. The impact charge distribution is reminiscent of three individual particle populations: small particles with impact charges $Q_1 < 10^{-13}$ C (AR1), intermediate par-

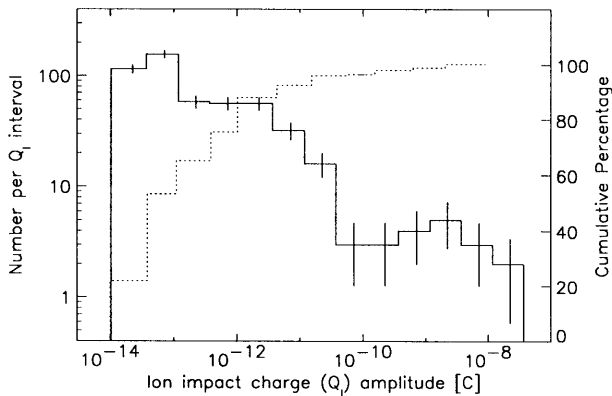


Fig. 4. Distribution of the impact charge amplitude Q_1 for all particles detected between 1993–95. The solid line indicates the number of impacts per charge interval, and the dotted line shows the cumulative percentage. Vertical bars indicate the \sqrt{n} statistical error.

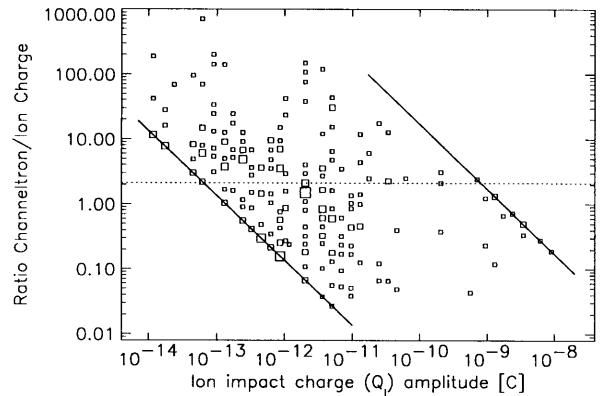


Fig. 5. Channeltron amplification factor $A = Q_c/Q_1$ as a function of impact charge Q_1 for all particles detected between 1993–95. The solid lines denote the sensitivity threshold (lower left) and the saturation limit (upper right) of the channeltron. Squares indicate dust particle impacts. The area of each square is proportional to the number of events included (the scaling of the squares differs from that used in Paper III). The dotted horizontal line shows the mean value of the channeltron amplification $A = 2.1$ for ion impact charges 10^{-12} C < Q_1 < 10^{-11} C.

ticles with 10^{-13} C $\leq Q_1 \leq 3 \times 10^{-11}$ C (AR2 and AR3) and big particles with $Q_1 > 3 \times 10^{-11}$ C (AR4 to AR6). The intermediate particles are mostly of interstellar origin and the big particles are interplanetary particles detected close to the ecliptic plane (Grün et al., 1997; see also Section 5). The small particles occur mostly over the Sun’s polar regions and are attributed to a population of interplanetary β -meteoroids at high ecliptic latitudes (Baguhl et al., 1995b; Hamilton et al., 1996).

The ratio of the channeltron charge Q_c and the ion collector charge Q_1 is a measure of the channeltron amplification A . The channeltron amplification is an important parameter for dust impact identification (Paper I). In Fig. 5 we show the charge ratio Q_c/Q_1 as a function of Q_1 for the nominal high voltage of 1140 V ($HV = 3$). The mean amplification determined from particles with 10^{-12} C $\leq Q_1 \leq 10^{-11}$ C is $A \approx 2.1$. This is very close to the value obtained in Paper III for the first two years of the

mission ($A \approx 2.2$). Therefore, the channeltron does not show any detectable aging during the more than five years of the Ulysses mission.

Figure 6 shows the masses and velocities of all dust particles detected between 1993–95. As in the earlier period (1990–92; Paper III), velocities occur over the entire calibrated range from 2–70 km/s. The masses vary over 10 orders of magnitude from 10^{-6} g– 10^{-16} g. The mean errors are a factor of 2 for the velocity and a factor of 10 for the mass. The clustering of the velocity values is due to discrete steps in the rise time measurement but this quantization is much smaller than the velocity uncertainty. For many particles in the lowest two amplitude ranges (AR1 and AR2) the velocity had to be computed from the ion charge signal alone which leads to the striping in the lower mass range in Fig. 6 (most prominent above 10 km s⁻¹). In the higher amplitude ranges the velocity could normally be calculated from both the target and the ion charge signal, resulting in a more continuous distribution in the mass-velocity plane. Impact velocities below about 3 km/s should be treated with caution because anomalous impacts onto the sensor grids or structures other than the target generally lead to prolonged rise times and hence to unnaturally low impact velocities.

5. Discussion

Most of the time from January 1993–December 1995, Ulysses was at high ecliptic latitudes far away from the ecliptic plane. The dust impact rate detected by the Ulysses dust sensor in this period is displayed in Fig. 7. The highest overall impact rate was detected around the

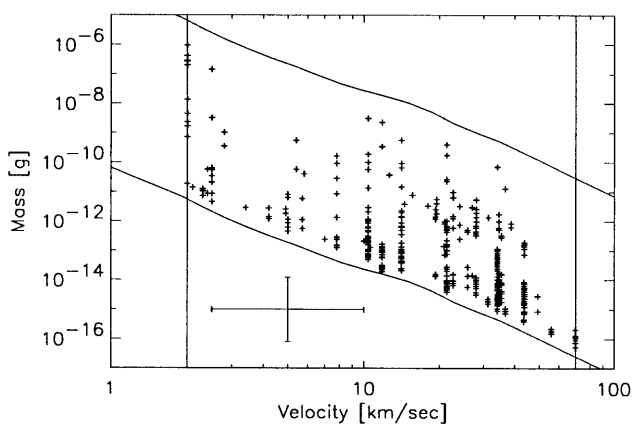


Fig. 6. Masses and impact velocities of all impacts recorded with the Ulysses sensor between 1993–95. The lower and upper solid lines indicate the threshold and the saturation limit of the detector, respectively, and the vertical lines indicate the calibrated velocity range. A sample error bar is shown that indicates a factor of 2 uncertainty for the velocity and a factor of 10 for the mass determination.

ecliptic plane crossing which occurred on 12 March 1995 (at 1.3 AU from the Sun). The maximum impact rate of particles in the three highest ion amplitude ranges (AR4 to AR6) coincides with the highest overall impact rate (upper panel of Fig. 7). These impacts are attributed to interplanetary particles on low inclination orbits (Grün et al., 1997). These are the impacts with $Q_1 > 10^{-10}$ C shown in Fig. 4. The impact rate of particles in the lowest amplitude range (AR1) increased gradually since mid 1993, reached its maximum at the ecliptic plane crossing in March 1995 and decreased later. Although the impact rate reached its maximum during a short time around the ecliptic plane crossing, the majority of these small particles has been detected during the much longer time interval when Ulysses was at high ecliptic latitudes. They are attributed to a population of small interplanetary particles on escape trajectories from the solar system (Baguhl et al., 1995; Hamilton et al., 1996).

The impact rate of particles in the intermediate ion amplitude ranges AR2 and AR3 was relatively constant during the 1993–95 period. It dominated the overall impact rate until early 1994, i.e., outside about 3.5 AU

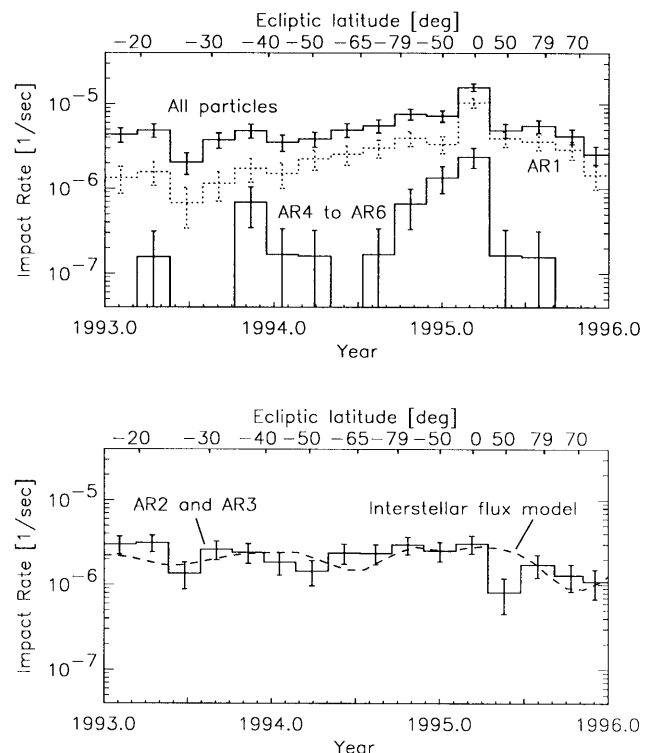


Fig. 7. Impact rate of dust particles detected with the Ulysses dust sensor as a function of time with the ecliptic latitude of the spacecraft indicated at the top. Upper panel: the upper solid line shows the total impact rate, the dotted line the impact rate of small particles (AR1) and the lower solid line the rate of big particles (AR4–AR6). Note that a rate of about 1.8×10^{-7} impacts per second is caused by a single dust impact in the averaging interval of about 70 days. Lower panel: intermediate particles (AR2 and AR3, solid line). A model for the rate of interstellar particles assuming a constant flux is superimposed as a dashed line.

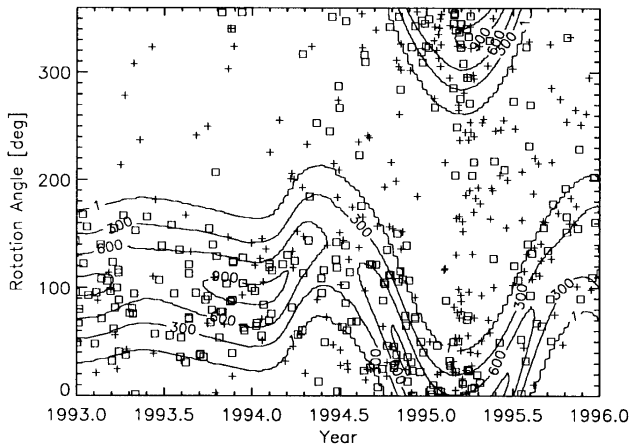


Fig. 8. Rotation angle vs time for all particles detected between 1993–95 for which complete information is available. Plus signs indicate particles with impact charge $Q_I < 8 \times 10^{-14}$ C, squares those with $Q_I \geq 8 \times 10^{-14}$ C. The contour lines show the sensitive area of the dust sensor for particles approaching from the interstellar upstream direction (levels of 1, 300, 600 and 900 cm^2 detector area are shown). Most of the larger Q_I particles came from directions consistent with the interstellar upstream direction. The biggest particles in the highest amplitude ranges which are of interplanetary origin are not shown separately here because only very few of them were detected (cf. Table 2) and they cannot be separated from interstellar particles by directional arguments. passage over the Sun's south polar region occurred in October 1994, ecliptic plane crossing in March 1995, and passage over the Sun's north polar region in August 1995.

from the Sun. Impacts in these ion amplitude ranges are mostly due to interstellar particles (see also Fig. 8 and Grün et al., 1993; Baguhl et al., 1995). Figure 7 also shows the expected impact rate of interstellar particles assuming that they approach from the direction of interstellar helium (Witte et al., 1996) and that they move on straight trajectories with a relative velocity of 26 km s^{-1} through the solar system. This assumption means dynamically that radiation pressure cancels gravity for these particles ($\beta = 1$) and that their Larmor radii are large compared with the dimension of the solar system. Both assumptions are reasonable for particles with masses between 10^{-13} – 10^{-12} g which is the dominant size range measured for interstellar particles (e.g., Grün et al., 1997). The dust particle flux is independent of heliocentric distance in this simple model, which gives relatively good agreement with the observed impact rate. The variation predicted by the model is caused by changes in the instrument's viewing direction with respect to the approach direction of the particles and changes in the relative velocity between the spacecraft and the particles. After the ecliptic plane crossing the rate of interstellar particles expected from the model is significantly higher than the one observed. A detailed dynamical model (Landgraf, 1998) for the motion of interstellar particles in the inter-

planetary magnetic field gives better agreement with the observed impact rate, especially after 1996.

The sensor orientation at the time of a particle impact (rotation angle) is shown in Fig. 8. The detector's sensitive area for particles approaching from the interstellar direction is superimposed. The bigger particles (squares, impact charge $Q_I \geq 8 \times 10^{-14}$ C) are clearly concentrated towards the interstellar direction. They have been detected with a relatively constant rate during the whole three-year period (Fig. 7). Only a few small particles (crosses, impact charges $Q_I \leq 8 \times 10^{-14}$ C) have been detected and they cluster above the Sun's polar regions. The particles with the highest ion amplitude ranges (AR4–AR6) are not distinguished in this diagram because they cannot be separated from interstellar particles by directional arguments. They have to be distinguished by other means (e.g., mass and velocity). Furthermore, their total number is so small that they constitute only a small 'contamination' of the interstellar particles in Fig. 8. In the ecliptic plane at 1.3 AU, however, interplanetary particle flux dominates over interstellar flux by a factor of about 3 (in number).

Streams of tiny dust particles originating from the Jovian system have been first detected with Ulysses and later with Galileo out to 2 AU from Jupiter (Grün et al., 1993, 1996). During the time period from 1993–95 considered here, Ulysses was more than 2.5 AU away from Jupiter which makes a significant contribution of Jovian dust stream particles in the present data set very unlikely. Analysis of the particles' trajectories and their interaction with the interplanetary magnetic field (Zook et al., 1996) showed that the velocities are about 300 km/s and the particles are about 10 nm in size. These values are far beyond the calibrated range of the dust sensors given above and, in principle, one cannot exclude that the data set presented in this paper contains at least a fraction of particles for which the masses and velocities inferred from our calibration are wrong. Recent analyses of the interplanetary (Grün and Staubach, 1997) and interstellar populations (Landgraf, 1998), however, are consistent with the calibrated velocities and masses of the particles in the new 1993–95 data set. Given the present knowledge about the particles' dynamics, the velocities and masses stated in Papers II and III for the stream particles are not correct. Future investigations will address possible contributions of particles beyond the calibrated range of the dust instruments in the complete Ulysses and Galileo data sets, not only close to Jupiter where the dust streams have been detected.

Acknowledgements

This work has been supported by the Deutsche Agentur für Raumfahrtangelegenheiten (DARA).

References

- Baguhl, M., Grün, E., Linkert, D., Linkert, G., Siddique, N., 1993. Identification of 'small' dust impacts in the Ulysses dust detector data. *Planet. Space Sci.* 41, 1085–1098.
- Baguhl, M., Grün, E., Hamilton, D.P., Linkert, G., Riemann, R., Staubach, P., Zook, H., 1995a. The flux of interstellar dust observed by Ulysses and Galileo. *Space Sci. Rev.* 72, 471–476.
- Baguhl, M., Hamilton, D.P., Grün, E., Dermott, S., Fechtig, H., Hanner, M.S., Kissel, J., Lindblad, B.-A., Linkert, D., Linkert, G., Mann, I., McDonnell, J.A.M., Morfill, G.E., Polansky, C., Riemann, R., Schwehm, G., Staubach, P., Zook, H., 1995b. Dust measurements at high ecliptic latitudes. *Science* 268, 1016–1019.
- Baguhl, M., Grün, E., Landgraf, M., 1996. In situ measurements of interstellar dust with the Ulysses and Galileo spaceprobes. *Space Sci. Rev.* 78, 165–172.
- Divine, N., 1993. Five populations of interplanetary meteoroids. *J. Geophys. Res.* 98, 17,029–17,048.
- Divine, N., Grün, E., Staubach, P., 1993. Modelling the meteoroid distributions in interplanetary space and near Earth. In: Flury, W. (Ed.). *Proceedings of the First European Conference on Space Debris*. Darmstadt, ESA SD-01, pp. 245–250.
- Grün, E., 1994. Dust measurements in the outer solar system. In: Melani, A., Di Martino, M., Cellino, A. (Eds.). *Asteroids, Comets, Meteors 1993*. Kluwer Acad. Publ., pp. 367–380.
- Grün, E., Fechtig, H., Hanner, M.S., Kissel, J., Lindblad, B.-A., Linkert, D., Linkert, G., Morfill, G.E., Zook, H.A., 1992a. The Galileo dust detector. *Space Sci. Rev.* 60, 317–340.
- Grün, E., Fechtig, H., Giese, R.H., Kissel, J., Linkert, D., Maas, D., McDonnell, J.A.M., Morfill, G.E., Schwehm, G., Zook, H.A., 1992b. The Ulysses dust experiment. *Astron. Astrophys. Suppl. Ser.* 92, 411–423.
- Grün, E., Baguhl, M., Fechtig, H., Hanner, M.S., Kissel, J., Lindblad, B.-A., Linkert, D., Linkert, G., Mann, I., McDonnell, J.A.M., Morfill, G.E., Polansky, C., Riemann, R., Schwehm, G., Siddique, N., Zook, H.A., 1992c. Galileo and Ulysses dust measurements: From Venus to Jupiter. *Geophys. Res. Letters* 19, 1311–1314.
- Grün, E., Zook, H.A., Baguhl, M., Fechtig, H., Hanner, M.S., Kissel, J., Lindblad, B.-A., Linkert, D., Linkert, G., Mann, I., McDonnell, J.A.M., Morfill, G.E., Polansky, C., Riemann, R., Schwehm, G., Siddique, N., 1992d. Ulysses dust measurements near Jupiter. *Science* 257, 1550–1552.
- Grün, E., Zook, H.A., Baguhl, M., Balogh, A., Bame, S.J., Fechtig, H., Forsyth, R., Hanner, M.S., Horanyi, M., Kissel, J., Lindblad, B.-A., Linkert, D., Linkert, G., Mann, I., McDonnell, J.A.M., Morfill, G.E., Phillips, J.L., Polansky, C., Schwehm, G., Siddique, N., Staubach, P., Svestka, J., Taylor, A., 1993. Discovery of jovian dust streams and interstellar grains by the Ulysses spacecraft. *Nature* 362, 428–430.
- Grün, E., Hamilton, D.P., Baguhl, M., Riemann, R., Horanyi, M., Polansky, C., 1994a. Dust streams from comet Shoemaker-Levy 9? *Geophys. Res. Lett.* 21, 1035–1038.
- Grün, E., Gustafson, B., Mann, I., Baguhl, M., Morfill, G.E., Staubach, P., Taylor, A., Zook, H.A., 1994b. Interstellar dust in the heliosphere. *Astron. Astrophys.* 286, 915–924.
- Grün, E., Baguhl, M., Fechtig, H., Hamilton, D.P., Kissel, J., Linkert, D., Linkert, G., Riemann, R., 1995a (Paper I). Reduction of Galileo and Ulysses dust data. *Planet. Space Sci.* 43, 941–951.
- Grün, E., Baguhl, M., Divine, N., Fechtig, H., Hamilton, D.P., Hanner, M.S., Kissel, J., Lindblad, B.-A., Linkert, D., Linkert, G., Mann, I., McDonnell, J.A.M., Morfill, G.E., Polansky, C., Riemann, R., Schwehm, G., Siddique, N., Staubach, P., Zook, H.A., 1995b (Paper II). Three years of Galileo dust data. *Planet. Space Sci.* 43, 953–969.
- Grün, E., Baguhl, M., Divine, N., Fechtig, H., Hamilton, D.P., Hanner, M.S., Kissel, J., Lindblad, B.-A., Linkert, D., Linkert, G., Mann, I., McDonnell, J.A.M., Morfill, G.E., Polansky, C., Riemann, R., Schwehm, G., Siddique, N., Staubach, P., Zook, H.A., 1995c (Paper III). Two years of Ulysses dust data. *Planet. Space Sci.* 43, 971–999.
- Grün, E., Staubach, P., 1996. Dynamic populations of dust in interplanetary space. In: Gustafson, B.A., Hanner, M.S. (Eds.). *Physics, Chemistry and Dynamics of Interplanetary Dust*. ASP Conference Series, vol. 104, pp. 3–14.
- Grün, E., Baguhl, M., Hamilton, D.P., Riemann, R., Zook, H.A., Dermott, S., Fechtig, H., Gustafson, B.A., Hanner, M.S., Horányi, M., Khurana, K.K., Kissel, J., Kivelson, M., Lindblad, B.-A., Linkert, D., Linkert, G., Mann, I., McDonnell, J.A.M., Morfill, G.E., Polansky, C., Schwehm, G., Srama, R., 1996. Constraints from Galileo observations on the origin of jovian dust streams. *Nature* 381, 395–398.
- Grün, E., Staubach, P., Baguhl, M., Hamilton, D.P., Zook, H.A., Dermott, S., Gustafson, B.A., Fechtig, H., Kissel, J., Linkert, D., Linkert, G., Srama, R., Hanner, M.S., Polansky, C., Horanyi, M., Lindblad, B.-A., Mann, I., McDonnell, J.A.M., Morfill, G.E., Schwehm, G., 1997. South-north and radial traverses through the zodiacal cloud. *Icarus* 129, 270–288.
- Hamilton, D.P., Burns, J.A., 1992. Orbital stability zones about asteroids II. The destabilizing effects of eccentric orbits and of solar radiation. *Icarus* 96, 43–64.
- Hamilton, D.P., Burns, J.A., 1993. Ejection of dust from Jupiter's gossamer ring. *Nature* 364, 695–699.
- Hamilton, D.P., Grün, E., Baguhl, M., 1996. Electromagnetic escape of dust from the Solar System. In: Gustafson, B.A., Hanner, M.S. (Eds.). *Physics, Chemistry and Dynamics of Interplanetary Dust*. ASP Conference Series, vol. 104, pp. 31–34.
- Horanyi, M., Grün, E., Morfill, G.E., 1993a. Mechanism for the acceleration and ejection of dust grains from Jupiter's magnetosphere. *Nature* 363, 144–146.
- Horanyi, M., Grün, E., Morfill, G.E., 1993b. The dusty ballerina skirt of Jupiter. *J. Geophys. Res.* 98, 21,245–21,251.
- Krüger, H., Grün, E., Hamilton, D.P., Baguhl, M., Dermott, S., Fechtig, H., Gustafson, B.A., Hanner, M.S., Horányi, M., Kissel, J., Lindblad, B.-A., Linkert, D., Linkert, G., Mann, I., McDonnell, J.A.M., Morfill, G.E., Polansky, C., Riemann, R., Schwehm, G., Srama, R., Zook, H.A., 1998 (Paper IV). Three years of Galileo dust data II: 1993 to 1995. *Planet. Space Sci.*
- Landgraf, M., 1998. Modellierung der Dynamik und Interpretation der In-Situ-Messung interstellarer Staubs in der lokalen Umgebung des Sonnensystems. Ph.D. thesis, University of Heidelberg.
- Landgraf, M., Grün, E., 1998. In situ measurements of interstellar dust. In: Breitschwerdt, D., Freyberg, M.J., Trümper, J. (Eds.). *Proceedings of the IAU Colloquium No. 166 on the Local Bubble and Beyond*. Lecture Notes in Physics, vol. 506. Springer, Heidelberg, pp. 381–384.
- Mann, I., Grün, E., Baguhl, M., Fechtig, H., Hanner, M.S., Kissel, J., Lindblad, B.-A., Linkert, D., McDonnell, J.A.M., Morfill, G.E., Polansky, C., Riemann, R., Schwehm, G., Siddique, N., Zook, H.A., 1992. Measurements with the Ulysses and Galileo dust detectors close to the ecliptic. In: *Proceedings of the 30th Liege international astrophysical colloquium 'Observations and physical properties of small solar system bodies'*, June 1992, Univ. de Liege, Institut d'Astrophysique, pp. 13–17.
- Mann, I., Grün, E., 1993.
- Mann, I., Grün, E., 1995. Dust particles beyond the asteroid belt—a study based on recent results of the Ulysses dust experiment. *Planet. Space Sci.* 43, 827–832.
- Mann, I., Grün, E., Wilk, M., 1996a. The contribution of asteroid dust to the interplanetary dust cloud: The impact of Ulysses results on the understanding of dust production in the asteroid belt and the formation of the IRAS dust bands. *Icarus* 120, 399–407.
- Mann, I., Wilk, M., Grün, E., 1996b. Analysis of Ulysses dust measurements within the asteroid belt. In: Gustafson, B.A., Hanner, M.S. (Eds.). *Physics, Chemistry and Dynamics of Interplanetary Dust*. ASP Conference Series, vol. 104, pp. 19–22.

- Riemann, R., Grün, E., 1992. Meteor streams, asteroids and comets near the orbits of Galileo and Ulysses. In: McDonnell, J.A.M. (Ed.). *Proceeding of the workshop on Hypervelocity Impacts in Space*. University of Kent at Canterbury, pp. 120–125.
- Stone, R.G., Bougeret, J.L., Caldwell, J., Canu, P., de Conchy, Y., Cornilleau-Wehrin, N., Desch, M.D., Fainberg, J., Goetz, K., Goldstein, M.L., Harvey, C.C., Hoang, S., Howard, R., Kaiser, M.L., Kellogg, P., Klein, B., Knoll, R., Lecacheux, A., Langyel-Frey, D., MacDowall, R.J., Manning, R., Meetre, C.A., Meyeer, A., Monge, N., Monson, S., Nicol, G., Reiner, M.J., Steinbert, J.L., Torres, E., de Villedary, C., Wouters, F., Zarka, P., 1992. The unified radio and plasma wave investigation. *Astron. Astrophys. Suppl. Ser.* 92, 291–316.
- Svestka, J., Auer, S., Baguhl, M., Grün, E., 1996. Measurements of dust electric charges by the Ulysses and Galileo dust detectors. In: Gustafson, B.A., Hanner, M.S., (Eds.). *Physics, Chemistry and Dynamics of Interplanetary Dust*. ASP Conference Series, vol. 104, pp. 31–34.
- Taylor, A.D., McDonnell, J.A.M., Grün, E., 1996. Taurid complex meteoroids detected near aphelion with Ulysses. *Adv. Space Res.* 17 (12) 171–175.
- Wenzel, K.P., Marsden, R.G., Page, D.E., Smith, E.J., 1992. The Ulysses mission. *Astron. Astrophys. Suppl. Ser.* 92, 207–219.
- Witte, M., Banaszekiewicz, H., Rosenbauer, H., 1996. Recent results on the parameters of interstellar helium from the Ulysses/GAS experiment. *Space Sci. Rev.* 78, No. 1/2, 289–296.
- Zook, H.A., Grün, E., Baguhl, M., Hamilton, D.P., Linkert, G., Liou, J.-C., Forsyth, R., Phillips, J.L., 1996. Solar wind magnetic field bending of jovian dust trajectories. *Science* 274, 1501–1503.